

Quartz Tuning Fork: Thermometer, Pressure- and Viscometer for Helium Liquids*

R. Blaauwgeers,¹ M. Blazkova,² M. Človečko,³ V.B. Eltsov,^{1,4}
R. de Graaf,¹ J. Hosio,¹ M. Krusius,¹ D. Schmoranzer,⁵ W. Schoepe,⁶
L. Skrbek,^{2,5} P. Skyba,³ R.E. Solntsev,¹ and D.E. Zmeev^{1,4}

¹Low Temperature Laboratory, Helsinki University of Technology, Espoo, Finland
E-mail: ve@boojum.hut.fi, mkrusius@neuro.hut.fi

²Institute of Physics ASCR, Na Slovance 2, 182 21 Prague, Czech Republic

³Centre of Low Temperature Physics, Institute of Experimental Physics SAV, Košice, Slovakia

⁴Kapitza Institute for Physical Problems, Kosygina 2, Moscow 119334, Russia

⁵Faculty of Mathematics and Physics, Charles University, Ke Karlovu 3, 121 16 Prague, Czech Republic

⁶Fakultät für Physik, Universität Regensburg, D-93040 Regensburg, Germany

Commercial quartz oscillators of the tuning-fork type with a resonant frequency of ~ 32 kHz have been investigated in helium liquids. The oscillators are found to have at best Q values in the range 10^5 – 10^6 , when measured in vacuum below 1.5 K. However, the variability is large and for very low temperature operation the sensor has to be preselected. We explore their properties in the regime of linear viscous hydrodynamic response in normal and superfluid ^3He and ^4He , by comparing measurements to the hydrodynamic model of the sensor.

PACS Numbers: 47.80.−v; 67.90.+z; 85.50.−n.

1. INTRODUCTION

Quartz tuning forks are commercially produced piezoelectric oscillators meant to be used as frequency standards in watches. An extensive literature describes their use for a large number of other additional applications.¹ They have also been employed in liquid He temperature measurements.² This study was inspired by the expectation that industrially produced quartz

*Dedicated to former JLTP editor Frank Pobell.

oscillators, with a calibrated standard frequency of 2^{15} Hz (=32 768 Hz) at room temperature, would be reasonably identical and could be used as secondary thermometers without need for recalibration.

We have performed measurements on four different forks of identical dimensions, but produced by different manufacturers. It turns out that without preselection at LHe temperatures the results cannot be reduced on a common temperature dependence. For instance, the resonance width Δf_{vac} measured in vacuum below 1.5 K proved to be 0.06, 0.5, 1.4, and 0.06 Hz for these four sensors. This measure of the intrinsic dissipation, which limits the response of the device to its environment at the lowest temperatures, cannot be determined from room temperature measurements. It remains to be seen if simple preselection criteria can be worked out, to narrow down the variation in oscillator characteristics.

However, the quartz tuning fork offers other important advantages as a sensor of its cryogenic environment. Forks are cheap and readily available, they are robust and as such easy to install and to use, they operate at a higher frequency than most other vibrating sensors, and they are highly sensitive indicators of the physical properties of the medium in which they are immersed. Thus, they provide handy in situ information about the conditions in a sample container at the far end of a low-conductance filling line, which is helpful during flushing, filling, emptying, and in general, for reproducible monitoring of pressure and temperature changes. A major advantage in many applications is that to drive these piezoelectric devices no magnetic fields are needed and that they, in fact, are insensitive to them.^{3,2}

In this report, we explore the linear response of the quartz tuning fork in He liquids at low excitation, in the regime of viscous hydrodynamics. The purpose is to compare the measurements to a hydrodynamic model which could explain the measured results. For this Sec. 2 studies the oscillator properties of the tuning fork in vacuum. In Sec. 3, the influence of the surrounding medium is incorporated, Sec. 4 discusses briefly the practical measurement, and later sections describe the measured results in vacuum as well as in ^3He and ^4He liquids, by comparing the data to the physical model. We postpone to a later occasion the analysis of non-linear effects and of the lowest temperatures with collisionless motion of excitations. This latter aspect, the creation and detection of excitations and of quantized vortices in the $T \rightarrow 0$ temperature limit, is of great current interest. A large amount of new information has been discovered on vortex properties using vibrating resonators: (i) spheres,⁴ grids,⁵ and wires⁶ in $^4\text{He-II}$, (ii) grids⁷ and wires⁸ in $^3\text{He-B}$, and (iii) wires⁹ in $^3\text{He-}^4\text{He}$ mixtures. One might hope that the quartz tuning fork could be used for similar measurements.

2. CHARACTERISTICS OF THE VIBRATING TUNING FORK

2.1. Mechanical Properties

At sufficiently small oscillation amplitudes the fork can be described as a harmonic oscillator subject to a harmonic driving force $F = F_0 \cos(\omega t)$ and a drag force with linear dependence on velocity. The equation of motion is given by

$$\frac{d^2x}{dt^2} + \gamma \frac{dx}{dt} + \frac{k}{m}x = \frac{F}{m}. \quad (1)$$

We have here four parameters, namely the effective mass m (of one leg), the drag coefficient γ , the spring constant k , and the amplitude of the driving force F_0 . The effective mass and the drag coefficient depend on the medium around the oscillating fork. The solution of this differential equation is well known: It can be written as $x(t) = x_a(\omega) \sin(\omega t) + x_d(\omega) \cos(\omega t)$, where x_a and x_d are the absorption and dispersion, respectively. The mean absorbed power $\langle F dx/dt \rangle = F_0 \omega x_a/2$ is at maximum at the resonant frequency

$$\omega_0 = \sqrt{\frac{k}{m}}.$$

It is convenient to introduce the quality factor

$$Q = \frac{\omega_0}{\gamma}$$

as the ratio of the resonant frequency ω_0 to the frequency width $\Delta\omega = \gamma$, where $\Delta\omega$ is the full width of the resonance curve at half of the maximum power.

The geometry of the fork is sketched in Fig. 1. It is characterized by the length \mathcal{L} , width \mathcal{W} , and thickness \mathcal{T} of a leg. The relevant vibration mode is the basic antisymmetric mode, i.e., the one where the two legs of the fork move in antiphase along the direction of \mathcal{T} . Taking the known elasticity modulus E of quartz, $E = 7.87 \cdot 10^{10}$ N/m², the spring constant is given by¹⁰

$$k = \frac{E}{4} \mathcal{W} \left(\frac{\mathcal{T}}{\mathcal{L}} \right)^3$$

and the effective mass of one leg in vacuum is [10]

$$m_{\text{vac}} = 0.24267 \rho_q \mathcal{L} \mathcal{W} \mathcal{T}, \quad (2)$$

where we use for the density $\rho_q = 2659$ kg/m³, the density of quartz (neglecting the electrodes on the legs).

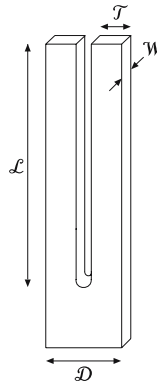


Fig. 1. Sketch of the quartz tuning fork.

We use forks with $\mathcal{L} = 3.12$ mm, $\mathcal{W} = 0.352$ mm, $\mathcal{T} = 0.402$ mm, and $\mathcal{D} = 1.0$ mm. For this geometry we find $k = 1.48 \cdot 10^4$ N/m and $m_{\text{vac}} = 2.85 \cdot 10^{-7}$ kg. This gives $f_0 = \omega_0/2\pi = 36293$ Hz, which is 11% larger than the manufactured value of 32768 Hz at room temperature. The discrepancy with the theoretical expression is most likely due to additional weight of the evaporated electrodes, dependence of the elasticity modulus of quartz on the orientation with respect to the crystallographic axes, and deviations in geometry between the real fork and the model. At room temperature in vacuum the measured width of the absorption curve at half power is typically $\Delta f \approx 1.2$ Hz, which gives $Q = f_0/\Delta f \approx 2.7 \cdot 10^4$. In room air the width increases to $\Delta f \approx 4.3$ Hz. With decreasing temperature the resonant frequency diminishes and the Q value increases. Our vacuum measurements at LHe temperatures will be presented in Sec. 5.

2.2. Electrical Properties and Calibration

The fork is excited with ac voltage $U = U_0 \cos(\omega t)$ while the frequency is slowly swept through resonance. The signal received from the fork is a current I owing to the piezoelectric effect. The stresses due to fork deflection induce charges and thus the current is proportional to the derivative of the fork deflection, i.e., to the velocity:

$$I(t) = a \frac{dx(t)}{dt}, \quad (3)$$

where a is the fork constant. Its theoretical value is given by¹¹

$$a = 3 d_{11} E (\mathcal{T} \mathcal{W} / \mathcal{L}), \quad (4)$$

where $d_{11} = 2.31 \cdot 10^{-12}$ m/V is the longitudinal piezoelectric modulus of quartz. For our forks $a = 2.47 \cdot 10^{-5}$ C/m. The oscillation amplitude is therefore known theoretically, but in practice the fork is usually calibrated optically with interferometric techniques.^{10,11,3} Typically, only *ca.* 30% of the theoretical current sensitivity is achieved. In a cryogenic setup, where the fork is mounted inside a sample container in the heart of the cryostat, a direct measurement of the fork constant a is complicated. Instead, we prefer to calibrate our forks by comparing the mechanical oscillator with the equivalent electrical RLC series resonance circuit.³ The corresponding differential equation for the current is

$$\frac{d^2 I}{dt^2} + \frac{R}{L} \frac{dI}{dt} + \frac{I}{LC} = \frac{1}{L} \frac{dU}{dt}. \quad (5)$$

Comparing Eqs. (5) and (1) we see that $\omega_0^2 = 1/(LC)$, $\gamma = R/L$, and using Eq. (3), $1/L = (F_0/U_0) a/m$. Additionally we have the condition that the dissipated power at resonance has to be equal for both equations: The electrical power $U_0^2/(2R)$ drives two legs of the fork which dissipate $2 \cdot F_0^2/(2m\gamma)$. Thus, we have a closed set of equations which allows us to connect the electrical and mechanical properties of the fork via the fork constant a :

$$F_0 = (a/2) U_0, \quad (6)$$

$$R = 2m\gamma/a^2, \quad (7)$$

$$L = 2m/a^2, \quad (8)$$

$$C = a^2/(2k). \quad (9)$$

Experimentally the fork constant a can be determined using Eq. (7), which, noting that $\gamma = \Delta\omega$, can be rewritten as

$$a = \sqrt{\frac{2m \Delta\omega}{R}}. \quad (10)$$

Here $\Delta\omega$ is determined from the width of the resonance curve while $1/R$ is the linear slope of the experimental $I_0(U_0)$ dependence, where I_0 is the current amplitude at resonance. The only parameter which cannot be directly determined from the experiment is the effective mass m . However the theoretical value of the effective mass (Eq. (2)) seems to be fairly reliable because of the close agreement between theoretical and experimental values of the resonant frequency. The example of our fork response in vacuum in Sec. 5 leads to $a = 8.13 \cdot 10^{-6}$ C/m, which amounts to 33% of the theoretical value.

In our experiment, the absorption $I_a(\omega)$ and dispersion $I_d(\omega)$ components of the current $I(t) = I_a \cos(\omega t) + I_d \sin(\omega t)$ are measured separately

with a lock-in amplifier (see Sec. 4 for details). The theoretical resonance curves,

$$I_a = \frac{a^2 U_0}{2} \frac{m\gamma\omega^2}{(m\gamma\omega)^2 + (m\omega^2 - k)^2} = \frac{I_0(\Delta\omega)^2\omega^2}{(\Delta\omega)^2\omega^2 + (\omega^2 - \omega_0^2)^2}, \quad (11)$$

$$I_d = \frac{a^2 U_0}{2} \frac{\omega(m\omega^2 - k)}{(m\gamma\omega)^2 + (m\omega^2 - k)^2} = \frac{I_0\Delta\omega\omega(\omega^2 - \omega_0^2)}{(\Delta\omega)^2\omega^2 + (\omega^2 - \omega_0^2)^2} \quad (12)$$

can be fit to the experimental response to determine the parameters which enter Eq. (1). In particular, the absorption component $I_a(\omega)$ reaches its maximum value I_0 at a frequency which is exactly ω_0 and the full width $\Delta\omega$ of the absorption curve at 1/2 of the maximum height I_0 gives exactly γ . If the fork constant a is known, then $m = a^2 U_0 / (2I_0 \Delta\omega)$ and $k = m\omega_0^2$ can be determined independently.

3. INFLUENCE OF SURROUNDING MEDIUM ON THE OSCILLATING FORK

3.1. Hydrodynamic Properties

In this section, we outline the basic properties of the oscillatory boundary layer flows, to understand how the vibrating fork works as a detector. The classical viscous flow around a submerged oscillating body¹² is rotational within a certain layer adjacent to the body, while at larger distances it rapidly changes to potential flow (if there is no free liquid surface or solid surface in the vicinity of the oscillating body). The depth of penetration of the rotational flow is of order

$$\delta = \sqrt{\frac{2\nu}{\omega}} = \sqrt{\frac{2\eta}{\rho\omega}}, \quad (13)$$

where ω is the angular frequency of oscillation while η and $\nu = \eta/\rho$ are the dynamic and kinematic viscosities of the fluid with density ρ .

As a result of the oscillatory motion of the body through the liquid, the body experiences a force which has components proportional to the velocity of the body v (drag) and to its acceleration \dot{v} (mass enhancement):

$$\mathcal{F} = bv + \tilde{m}\dot{v}. \quad (14)$$

To determine the values of b and \tilde{m} generally a full solution of the flow field around the oscillating body is required. Simplifications are possible in two limiting cases, which depend on the relative magnitudes of the characteristic size of the oscillating body ℓ , oscillation amplitude x_0 , and viscous penetration depth δ :

- (1) $\ell \ll \delta$ and $\omega x_0 \ell / \nu \ll 1$: In this case the flow at any given instant can be regarded as steady – as if the body were moving uniformly with its instantaneous velocity. As a rule, this case does not apply to the oscillating cryogenic flows considered here.
- (2) $\ell \gg \delta$ and $\ell \gg x_0$: In this case the layer of rotational flow around the body is very thin while in the rest of the fluid the flow is potential. This case is directly applicable to quartz tuning forks in ^3He and ^4He liquids: The kinematic viscosity of normal liquid $^4\text{He-I}$ above the λ -point is $\nu_4 \approx 2 \cdot 10^{-4} \text{ cm}^2/\text{s}$ and of normal ^3He above the superfluid transition $\nu_3 \approx 1 \text{ cm}^2/\text{s}$. At 32 kHz we get the penetration depths $\delta_4 \approx 0.4 \mu\text{m}$ and $\delta_3 \approx 30 \mu\text{m}$ while $\ell \approx 400 \mu\text{m}$ for our forks. Moreover, the oscillation amplitude would reach the leg thickness \mathcal{T} only at a very high velocity of order 1 m/s (cf. Fig. 6). Note that other oscillating objects, such as spheres or wires, may not always be in this flow regime since they usually have smaller characteristic size and smaller oscillation frequency.

When the conditions for case (2) above are valid, a major contribution to both b and \tilde{m} in Eq. (14) is found by solving the potential flow field u around the body.¹² In particular, b is expressed as

$$b = \sqrt{\frac{\rho\eta\omega}{2}} \left[\frac{1}{|v_0|^2} \oint |u_0|^2 dS \right] = \sqrt{\frac{\rho\eta\omega}{2}} C S, \quad (15)$$

where v_0 and u_0 are the amplitudes of the velocities of the body and the flow, the integral is taken over the surface of the oscillating body, S is the surface area of the body, and C is some numerical constant which depends on the exact geometry of the body. For example for a sphere $C = 3/2$, while for an infinitely long cylinder oscillating perpendicular to its axis $C = 2$.

The largest contribution to mass enhancement \tilde{m} comes from the potential flow around the body and can be expressed through the mass ρV of the liquid displaced by the body of volume V . A smaller contribution is caused by the fact that the viscous drag force experienced by the body is usually phase shifted with respect to the velocity of the body. This can be interpreted such that a volume of order $S\delta$ of the liquid is clamped to comotion with the oscillating body. Thus for \tilde{m} we can write

$$\tilde{m} = \beta\rho V + B\rho S\delta, \quad (16)$$

where β and B are again geometry-dependent coefficients. For example, for a sphere¹² $\beta = 1/2$ and $B = 3/4$; for an infinitely long cylinder with elliptic cross section¹³ $\beta = r_\perp/r_\parallel$, where r_\perp and r_\parallel are the lengths of the axes which are perpendicular and parallel to the oscillation direction,

respectively; for a rectangular beam¹⁴ $\beta = (\pi/4)a_{\perp}/a_{\parallel}$, where a_{\perp} and a_{\parallel} are the lengths of the sides which are perpendicular and parallel to the oscillation direction, respectively.

We are not aware of rigorous calculations of the parameters β , B , and \mathcal{C} for a tuning fork. A single oscillating beam has been considered before in great detail.¹⁴ However, the presence of two legs in close vicinity of each other significantly affects the potential flow field and changes, for example, the β parameter.² Thus, we consider β , B , and \mathcal{C} as fitting parameters, to be determined for a particular fork from the experiment. This approach was previously used, for example, in Ref. 15 for a vibrating reed in liquid ⁴He and it seems to provide the first step for understanding the experimental results.

3.2. Hydrodynamic Model of Sensor

The addition of the force \mathcal{F} to the equation of motion of the fork (1) leads to a reduction in the resonant frequency and an increase in the width of the resonance curve:

$$\omega_0^2 = \omega_{0\text{vac}}^2 (m_{\text{vac}}/m), \quad (17)$$

$$\gamma = \gamma_{\text{vac}}(m_{\text{vac}}/m) + b/m, \quad (18)$$

where $m = m_{\text{vac}} + \tilde{m}$ is the effective mass of the oscillating body immersed in the fluid. For convenience we redefine the fork parameters β and B from Eq. (16) as relative to the effective fork mass in vacuum:

$$\tilde{m} = m_{\text{vac}} \frac{\rho}{\rho_{\text{q}}} [\beta + B\delta(S/V)]. \quad (19)$$

Ignoring the vacuum resonance width Δf_{vac} , we finally obtain the dependence of the resonant frequency f_0 and of the full width of the absorption curve at half height Δf on the fluid density and viscosity:

$$\left(\frac{f_{0\text{vac}}}{f_0}\right)^2 = 1 + \frac{\rho}{\rho_{\text{q}}} \left(\beta + B \frac{S}{V} \sqrt{\frac{\eta}{\pi\rho f_0}}\right), \quad (20)$$

$$\Delta f = \frac{1}{2} \sqrt{\frac{\rho\eta f_0}{\pi}} \mathcal{C} S \frac{(f_0/f_{0\text{vac}})^2}{m_{\text{vac}}}. \quad (21)$$

Here $V = \mathcal{T}\mathcal{W}\mathcal{L}$ and $S = 2(\mathcal{T} + \mathcal{W})\mathcal{L}$.

Equations (20) and (21) can now be used to determine experimentally the hydrodynamic parameters from measurements in a fluid with known ρ and η . Once the parameters are known, the fork can be used for measurements of ρ and η , in principle, for any other medium and thus as a

pressure and temperature sensor, if $\rho(P, T)$ and $\eta(P, T)$ are known. From this point of view, the width Δf is especially useful for measurements as it requires calibration of only one parameter ($\mathcal{C}/m_{\text{vac}}$). In Eq. (20), the factor multiplying the parameter B is small and so, even here, often only one parameter (β) is of major importance. Unfortunately, our measurements indicate that the parameters vary from one fork to the next and calibrations need to be checked (see Secs. 6 and 7). The calibration should be re-examined even when performing measurements with the same fork in widely differing conditions (see Sec. 6).

3.3. Beyond the Model of Viscous Hydrodynamics

With decreasing temperature the mean free path of excitations increases in both ^4He and ^3He superfluids and the hydrodynamic description ceases to be valid as the normal fluid penetration depth grows beyond all relevant length scales. In $^4\text{He-II}$ the crossover to the ballistic regime takes place below 1 K and in $^3\text{He-B}$ below $0.3 T_c$. At low temperatures the drag is caused by the scattering of the excitations from the oscillating body. As the excitation density decreases with decreasing temperature the drag coefficient also rapidly decreases: $b \propto T^4$ for phonons in $^4\text{He-II}$, while $b \propto \exp(-\Delta/k_B T)$ for rotons and for quasiparticles in $^3\text{He-B}$, where Δ is the relevant energy gap. The crossover from the hydrodynamic to the ballistic regime has been described for a vibrating wire in Refs. 16,17 and for a vibrating sphere in Ref. 18. In this work, we are not discussing the ballistic regime further.

In everyday life a tuning fork is used to create sound in air. In the case of a quartz tuning fork in LHe we might wonder whether the compressibility and the losses from sound emission need to be taken into account. A quartz fork operates at higher frequency than vibrating wires, grids, spheres and most other oscillating bodies. Therefore, sound emission might be sizable for the fork while it is negligible in these other cases. The power loss from acoustic emission reduces the Q value and contributes to the width of the resonance curve $\Delta\omega_{\text{ac}} = R_{\text{ac}}/m$, where the average power loss $\frac{1}{2}R_{\text{ac}}v_0^2$ has been expressed in terms of the so-called radiation resistance R_{ac} .

A realistic calculation of the acoustic emission from a tuning fork is complicated. Clubb *et al.*² suggest a model of two infinite cylinders oscillating at 180° out-of-phase and give for their quadrupolar acoustic field the radiation resistance

$$R_{\text{ac}} = \frac{\pi^2 \omega^5 \rho \mathcal{W}^6 \mathcal{L}}{11616 c^4}. \quad (22)$$

This expression gives a very small contribution to the resonance width and, owing to the high powers in which the different quantities appear, quantitative comparison with experiment is so far inconclusive. In our measurements on normal ^3He a small temperature independent constant contribution to the resonance width is distinguishable at high temperatures (see Sec. 6). However, its magnitude is not in agreement with Eq. (22) and at this point the presence of the acoustic loss term remains unclear.

4. SENSOR PREPARATION AND MEASUREMENT

A commercial quartz tuning fork comes in a vacuum-tight sealed metal can which has to be partly or entirely removed, to probe the flow properties of the surrounding medium. The pair of leads for exciting and sensing the oscillator is magnetic. In magnetically sensitive applications they have to be removed and changed to nonmagnetic leads. For measuring the current in Eq. (5) one usually uses the current input of a phase-sensitive lock-in amplifier. The excitation voltage is supplied by a high-resolution digital generator, which also provides the reference signal for the lock-in amplifier (see circuit diagram in Fig. 2).

In Fig. 3, the results are plotted from room temperature test measurements, to compare to Eqs. (20) and (21). The measured nearly linear dependence of the resonant frequency and the square root dependence of the resonance width versus applied pressure P follow directly from these equations, assuming that $\rho \propto P$ and η does not appreciably change with P . In these measurements we also tested if the results showed variations depending on whether (i) only a small hole is made in the encapsulating can, or (ii) the entire top surface of the can is ground away, or (iii) the can is completely removed. No obvious qualitative differences were observed,

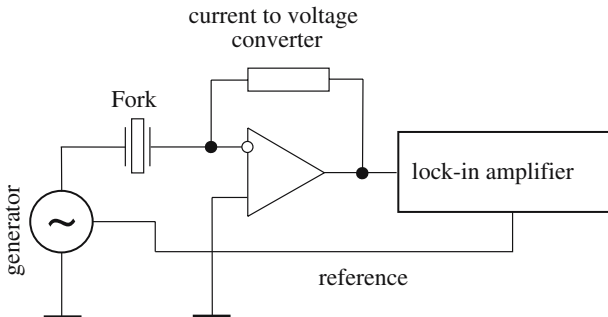


Fig. 2. Circuit diagram for tuning fork measurements.

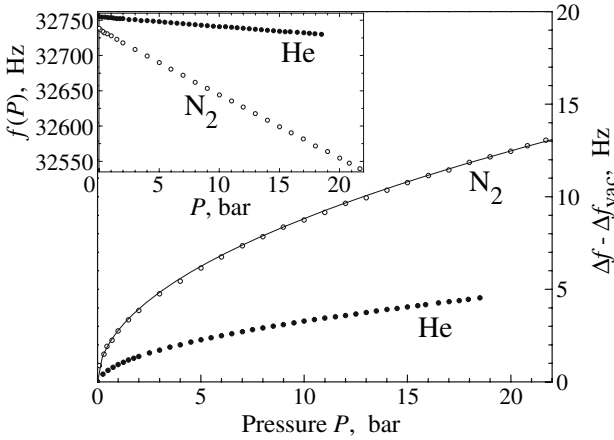


Fig. 3. Room temperature tests of sensor sensitivity. (*Main panel*) Resonance width Δf , with the vacuum width Δf_{vac} subtracted (right vertical scale), plotted versus applied pressure in gaseous nitrogen ($T = 22.5^\circ\text{C}$) and helium ($T = 23^\circ\text{C}$). The solid line is the fitted square root dependence, as expected from Eq. (21). (*Inset*) The corresponding resonant frequencies f_0 are almost linear with pressure, as expected from Eq. (20). The data for N_2 and He have been measured with two different forks.

which is as expected, since for all data in Fig. 3 the penetration depth δ is much smaller than the fork dimensions.

In Fig. 4, a similar measurement has been performed in liquid ^4He at 4.2 K as a function of pressure. Owing to the nonlinear dependence of the density of liquid He on applied pressure, the resonant frequency shows linear dependence only after converting pressures to densities. For these results thermal aging is of some concern. We tested the stability of the resonant frequency and width of five different forks by cycling them between 300 and 77 K, with their cans completely removed. For a virgin sensor resonant frequency shifts of $\lesssim 0.2\text{ Hz}$ and changes in width $\lesssim 0.3\text{ Hz}$ are typical. For most applications such shifts are negligible, but if more stable reproducible results are required, then the sensor should be thermally cycled. After a few cycles the changes are considerably reduced, but only after 30–50 cycles the results become stable. It should be noted that larger changes can result from bending the leads of the fork or from making new solderings to the leads, presumably because new strains are imposed via the electrodes on the quartz surface. Such changes, which can be $\lesssim 0.7\text{ Hz}$ in both resonant frequency and width, are generally larger than those caused by the removal of the can by grinding. This suggests that a fork, which is used as thermometer, should be handled with care.

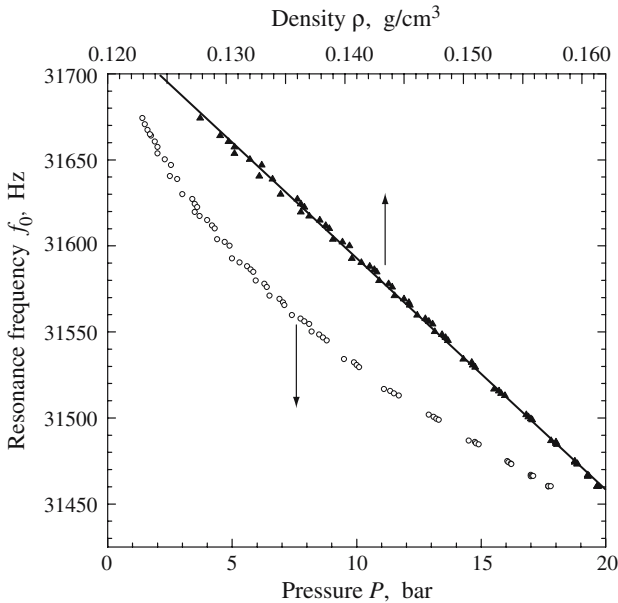


Fig. 4. Resonant frequency f_0 in liquid ^4He at 4.2K plotted versus applied pressure (bottom) and density (top). The tuning fork was in its original can, but with the flat top surface of the can ground away and $\Delta f_{\text{vac}} = 0.06$ Hz. The pressure was converted to density using the HEPAK package.¹⁹ The solid line is a linear fit through the data.

A further practical consideration in connection with Fig. 4 is that these results could only be obtained after the tuning fork was installed in an isolated sample container in controlled conditions. In a LHe bath in an open dewar surface conditions on the fork may change because of adsorbed gas or particles floating in the bath after a LHe transfer. Typically in such conditions the resonance width does not stay constant, but gradually increases during a long run. Occasionally small step changes in the resonant frequency are observed, which could arise if air flakes stick on the fork, for instance. Thus for accurate and reproducible readings the fork should preferably not be used in technical helium.

Figure 5 shows two examples of the quartz tuning fork as a practical monitoring device of temperatures in a nuclear cooling cryostat.^{20,21} The two traces illustrate the range which the resonance width Δf traverses when the cryostat is taken through its cooling cycle. The bottom trace represents a sensor in the mixing chamber, while the top trace monitors one on the nuclear cooling stage. The most prominent features in these traces are abrupt anomalies: In the bottom trace from disconnecting the super-

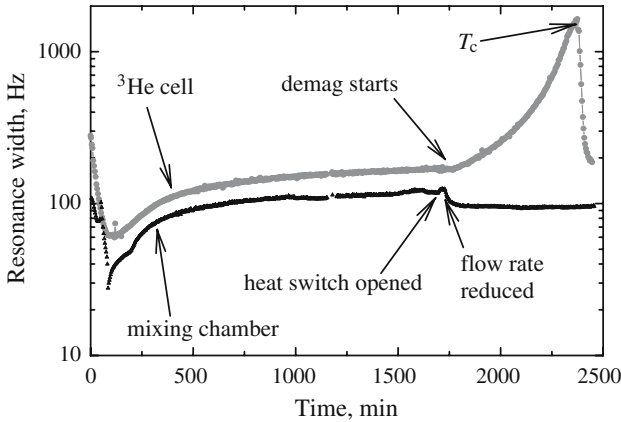


Fig. 5. Two quartz tuning forks monitoring temperatures in a nuclear cooling cryostat. The bottom trace shows the sensor inside the mixing chamber of the dilution refrigerator in the concentrated ^3He - ^4He solution. The top trace gives the simultaneously measured width of the sensor on the nuclear cooling stage inside the liquid ^3He sample container at zero liquid pressure.

conducting heat switch between the mixing chamber and the nuclear cooling stage. Here the mixing chamber first starts cooling, but then warms up to a new higher level when the ^3He flow rate in the dilution refrigerator circulation is reduced. Simultaneously, the demagnetization of the nuclear cooling stage is started. This means that in the upper trace the temperature starts decreasing and Δf increasing. When the cool down passes through the superfluid transition temperature T_c , the width suddenly dives in a rapid decrease (see Sec. 6). These recordings show that the quartz tuning fork provides rapid and sensitive confirmation of the actions which are performed on the cryostat.

5. PROPERTIES OF TUNING FORKS IN VACUUM

In its original package the quartz tuning fork comes inside a vacuum-tight can. When the fork is cooled in this can, the resonant frequency decreases and the Q value increases. At LHe temperatures the reduction in resonant frequency from the room-temperature value is about 70 Hz and the Q value approaches 10^6 . If the can is removed the bare fork behaves in vacuum in similar manner: The reduction in the resonant frequency remains the same while the Q value is typically lower than for the fork inside its original can. However, the Q value varies greatly from one fork to the next. Typical Q values range from $2 \cdot 10^4$ to $5 \cdot 10^5$. A similar large

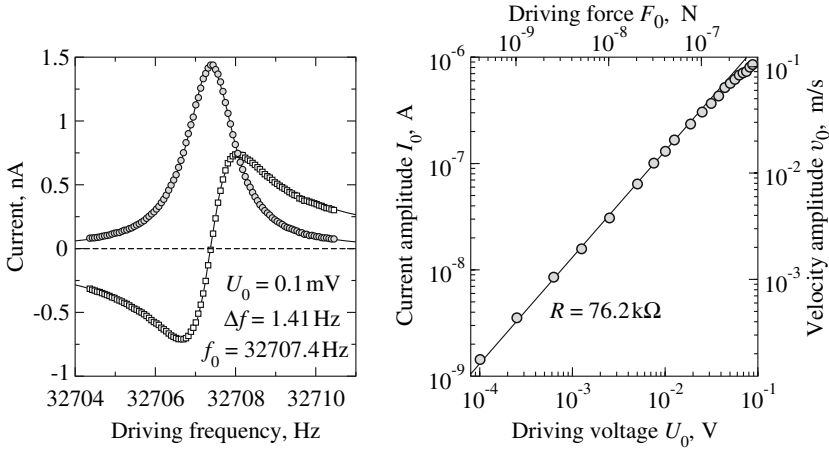


Fig. 6. Response of the quartz tuning fork in vacuum at a temperature of about 1 K. (*Left*) Resonance curves for absorption I_a (\circ) and dispersion I_d (\square) components of the current measured at fixed excitation level U_0 . The solid curves are fits to Eqs. (11) and (12). Background contributions from a shunting capacitance and leads are subtracted. (*Right*) Dependence of the amplitude I_0 of the current at resonance on the excitation voltage amplitude U_0 . Conversions to velocity and driving force via Eqs. (3) and (6) are also shown.

scatter was observed in previous reports.^{3,2} The reasons for such variability between different forks are not known. In principle differences may result from slight damage (when the can is removed, for instance) or from dirt accumulated on the legs. In practice of course, the resonance width is much larger in LHe than the vacuum width and thus these problems do not affect our later analysis. However, if one is interested in the properties at the lowest temperatures in the ballistic regime, then special care has to be invested in selecting forks with the narrowest possible vacuum width.

The vacuum response of a tuning fork at $\sim 1 \text{ K}$ is shown in Fig. 6. This fork was later used for measurements in ^3He liquid at zero pressure. The data in Fig. 6 were measured at different excitation levels in the ^3He sample container while the ^3He pressure was less than 1 mbar at a temperature of around 1 K. As mentioned above (Sec. 2.2), from the resonance characteristics measured at various excitation voltage amplitudes U_0 it is possible to determine the fork constant a using Eq. (10). In this case $a = 8.13 \cdot 10^{-6} \text{ C/m}$. Now the driving force F_0 and the velocity amplitude can be calculated from Eqs. (6) and (3), respectively. Thus the measurement of I_0 versus U_0 in the right panel of Fig. 6 can be converted to a dependence of the tuning fork velocity amplitude on the driving force.

As seen in Fig. 6, in vacuum the fork responds linearly up to a driving force of order 100 nN, which corresponds to displacements of a few μm . Above this limit the amplitude in the motion of the legs starts to be sufficient for the response to become nonlinear. The cause for the nonlinear behavior is deformation in the sensor material during large-amplitude oscillation. The oscillation amplitudes of ions around the minimum of their potential become large enough such that anharmonic terms in the potential energy introduce nonlinear restoring forces in the ion motion. The overall effect is the appearance of a nonlinear restoring force in the equation of motion, Eq. (1). In addition at low temperatures other sources contribute to nonlinearities in large amplitude oscillation, such as slow strain release from defects in the oscillator material. These have been extensively investigated, for instance with vibrating wire resonators in vacuum.²² The nonlinear drive regime of the quartz fork is not discussed in this report.

6. TUNING FORK IN ^3He

Our measurements in liquid ^3He have been performed in two different cryostats and with different sensors.²³ In the measurements at 29 bar pressure, the fork parameters were $f_{0\text{vac}} = 32705.05 \text{ Hz}$ and $\Delta f_{\text{vac}} = 0.06 \text{ Hz}$ in vacuum at LHe temperatures. In this setup temperatures above T_c are measured with a melting curve thermometer which is mounted on the nuclear cooling stage. Below T_c , the temperature readings are determined from nuclear magnetic resonance frequency shifts of the ^3He sample.²⁴ The NMR reading is preferred below T_c because it is measured directly from the liquid in which the tuning fork is also immersed. This minimizes thermal gradients between the thermometer and the fork.

In the zero pressure measurements the fork had $f_{0\text{vac}} = 32707.4 \text{ Hz}$ and $\Delta f_{\text{vac}} = 1.41 \text{ Hz}$. In this setup the temperature is determined with pulsed NMR on Pt powder immersed in the liquid ^3He sample. The NMR signal amplitude is calibrated using the known value of the superfluid ^3He transition temperature T_c . The superfluid transition is indicated by the fork reading or by two additional vibrating wire resonators in the ^3He cell, which also are used for thermometry.

The temperature dependence of the resonance width Δf at 29 bar pressure is presented in Fig. 7. The measurements were performed in the linear drive regime of the fork with the maximum current not exceeding 4 nA (and thus velocities not exceeding 0.18 mm/s). The plot demonstrates that the width changes rapidly in the range 0.8–40 mK and, once calibrated, can be used as a thermometer. The measurements were extended to much lower temperatures than shown in Fig. 7, the lowest observed

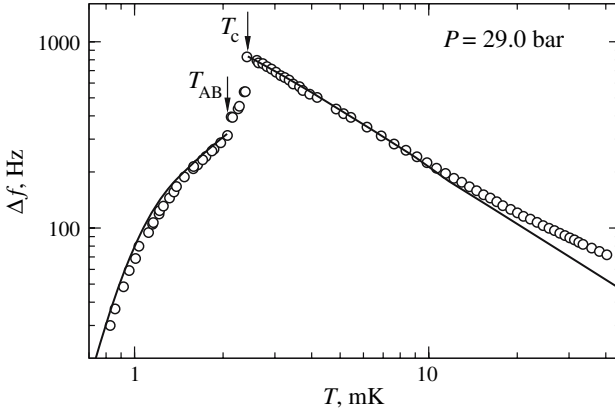


Fig. 7. Resonance width of the quartz tuning fork in liquid ${}^3\text{He}$ at 29 bar pressure. The measured data are marked with circles. A sharp reduction in the width is observed on cooling below T_c and an abrupt discontinuity at the AB transition. The solid line is the predicted behavior¹⁷ of a vibrating wire resonator with the same density ρ_q and the same vacuum resonant frequency $f_{0\text{vac}}$ as the fork. To produce a good fit to the quartz fork data the wire diameter had to be fixed to 0.25 mm which is comparable to the dimensions of the legs of the fork.

resonance width was $\Delta f = 0.18\text{ Hz}$. However, at these temperatures we have no other thermometer in the ${}^3\text{He}$ sample container to calibrate the fork.

Figure 7 can be divided in three temperature regimes: (i) normal ${}^3\text{He}$ above T_c , where the width rapidly increases with decreasing temperature due to the Fermi-liquid behavior of the viscosity, $\eta \propto 1/T^2$, (ii) superfluid ${}^3\text{He-A}$ and (iii) ${}^3\text{He-B}$ phases, where the width decreases with decreasing temperature mainly because of the decreasing normal-fluid density. Figure 7 provides an interesting comparison of the fork oscillator with the vibrating wire resonator. In Ref. 17, the available theoretical and experimental information on vibrating wires has been combined in a computer program which calculates the response of a vibrating wire loop in normal ${}^3\text{He}$ and in superfluid ${}^3\text{He-B}$ for a resonator with known wire diameter, wire density, and resonant frequency in vacuum. In Fig. 7, the response of a fictitious wire loop with the density of quartz and the frequency of the tuning fork in vacuum has been fitted to the experimental data with the wire diameter as a fitting parameter. The fit is remarkably good and gives a reasonable value for the wire diameter which is of order of the thickness of the fork leg. The same fit does not reproduce exactly the temperature dependence of the resonant frequency owing to the difference in the β factor between the wire and the fork (cf. Eqs. (20) and (21)). The comparison

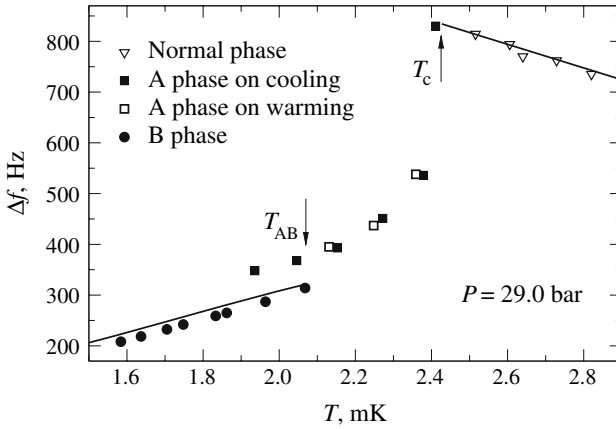


Fig. 8. Closeup of resonance width in Fig. 7 in the temperature region of ${}^3\text{He-A}$. During cooling the $\text{A} \rightarrow \text{B}$ transition is supercooled, while during warming the $\text{B} \rightarrow \text{A}$ transition occurs close to the thermodynamic equilibrium temperature T_{AB} of this first order phase transition. The discontinuous jump in resonance width at the transition is mainly caused by the change in ρ_n . The solid lines depict the vibrating wire model of Fig. 7.

is used here to emphasize that the fork thermometer is very comparable to the vibrating wire in this temperature range of liquid ${}^3\text{He}$.

Vibrating wires are generally not used as thermometers in ${}^3\text{He-A}$ owing to their texture-dependent nonreproducible response. Our limited experience with forks shows that for a given fork the width in the A phase is reproducible, independently whether one enters the A phase from the normal phase or from the B phase direction, as seen in Fig. 8. Probably the larger dimensions of the fork legs fix the orientations in the order parameter texture such that the response becomes reproducible if the oscillation amplitude remains small compared to the leg dimensions. Nevertheless, more measurements are required to establish whether tuning forks can be used as accurate secondary thermometers also in ${}^3\text{He-A}$.

In Fig. 9, the fork properties are analyzed in more detail in normal ${}^3\text{He}$. Since the viscosity of normal ${}^3\text{He}$ varies as $\eta \propto T^{-2}$, we expect the width to depend on temperature as $\Delta f \propto T^{-1}$, Eq. (21). This dependence is indeed observed in the experiment. However, a constant addition to the resonance width is also present in the experimental data (seen as a nonzero intercept on the vertical scale in the two panels of Fig. 9). This additional temperature-independent contribution to the width is 21.2 Hz at 29 bar and 3.2 Hz at zero pressure. In Fig. 7, this effect appears as a tendency toward a constant width at high temperatures.

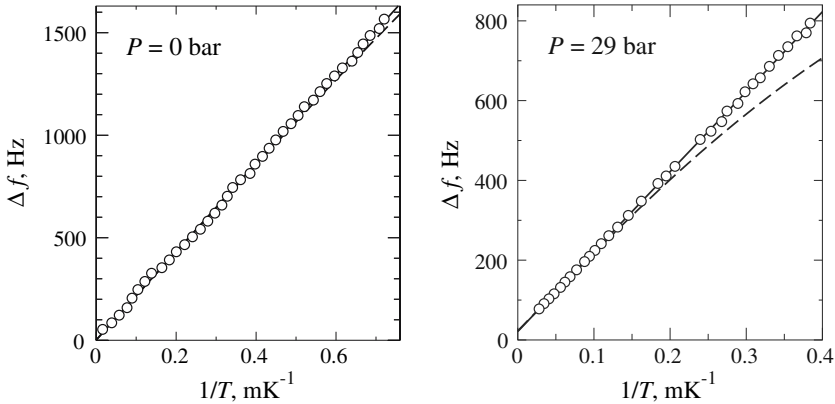


Fig. 9. Resonance width at two different pressures in normal ${}^3\text{He}$ as a function of inverse temperature. The experimental data is shown as circles. The solid lines are linear fits of Δf versus $1/T$. For comparison, the dashed curves show the effect from a viscosity anomaly close to T_c which was measured with a vibrating wire resonator in Ref. 25.

The origin of the temperature-independent contribution to the width in normal ${}^3\text{He}$ is not clear. Clubb *et al.*² observed the same effect in ${}^3\text{He}$ - ${}^4\text{He}$ mixtures and attributed it to acoustic emission. Their model, Eq. (22), gives orders of magnitude smaller value than the measured one in our case. Moreover, irrespectively of the model one would expect that the losses from sound emission will be smaller at high pressures (since the sound velocity increases with pressure), while the two measurements in Fig. 9 show opposite behavior. Since these have been performed with different sensors, the possibility remains at this point that the main part of the temperature independent width in normal liquid ${}^3\text{He}$ depends on the fork with which it is measured.

Several reports on vibrating wire measurements mention a viscosity anomaly in normal ${}^3\text{He}$: an unexpected reduction in the viscosity close to T_c from the T^{-2} behavior.²⁶ Our data show no sign of this anomaly: The width Δf changes exactly proportional to T^{-1} until T_c (Fig. 9). The reason for this difference is not clear. Possibly the fork owing to larger size and higher frequency operates in a different hydrodynamic regime than typical vibrating wire resonators. In particular close to T_c , where the viscosity of ${}^3\text{He}$ is the highest, the viscous penetration depth becomes comparable to the characteristic size of the oscillating object, especially at low pressure. For example for a fork at $P=0$ and $T=1$ mK, δ is about the inter-leg distance D . Thus an interpretation of the results in terms of the simple model presented in Sec. 3 may not be justified. The question which

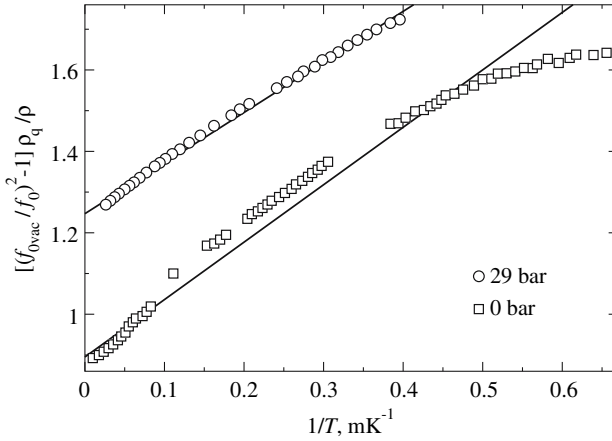


Fig. 10. Resonance frequencies of the two quartz tuning forks from Fig. 9 in normal ^3He , plotted as $[(f_{0\text{vac}}/f_0)^2 - 1]\rho_q/\rho$ versus $1/T$. The symbols represent experimental data. The solid lines are fits to Eq. (20), assuming $\eta \propto T^{-2}$.

kind of viscometer is more appropriate for ^3He at temperatures close to T_c requires further analysis.

From the linear fit in Fig. 9 the fork parameter C in Eq. (21) can be determined. Using viscosity data from Ref. 25 (omitting the viscosity anomaly close to T_c), we get $C=0.57$ for the fork used at zero pressure and $C=0.64$ for the fork used at 29 bar.

The relative change in the density of liquid ^3He between 0 and 40 mK is about 10^{-4} , according to Ref. 27. Thus, the largest contribution to the temperature dependence of the resonant frequency of the fork in this temperature range comes from the viscous mass enhancement in Eq. (20). Our experimental data for normal ^3He together with a fit to Eq. (20) are shown in Fig. 10. The quantity plotted on the vertical scale is the term in the parentheses on the right hand side of Eq. (20). The fit gives $\beta=0.90$ and $B=0.73$ for the mass enhancement parameters of the fork used at zero pressure and $\beta=1.25$ and $B=1.05$ for the fork used at 29 bar. The β factor can also be determined from measurements at the very lowest temperatures in $^3\text{He-B}$, well in the ballistic regime, when the shift of the resonant frequency is caused entirely by inertial effects. This way we obtain $\beta=0.88$ for the fork used at zero pressure and $\beta=1.20$ for the fork used at 29 bar. These second values are close to the ones shown as the zero intercepts on the vertical scale of Fig. 10.

We conclude that the mass enhancement factors β and B turn out to have rather different values for our two forks, in spite of the fact

that these two forks have closely similar dimensions and room-temperature oscillator properties. In both cases β is larger than the theoretical value $\beta = (\pi/4)\mathcal{W}/T = 0.69$ for a single beam of the size of one leg, as might be expected owing to the two legs of the fork in close vicinity of each other (Sec. 3.1). The sizeable differences in the fitted parameter values do not support our hopes that quartz tuning forks could be used as reproducible secondary thermometers, with a common calibration for all forks of the same type.

Another important question is whether for a given fork the calibration obtained for one pressure can be used to interpret results at another pressure without re-calibration. To check this we repeated measurements at zero pressure using the fork for which a calibration at $P = 29$ bar had been obtained. In the regime $\delta \ll (\mathcal{D}, T, \mathcal{W})$, where the simple model from Sec. 3.1 is applicable and which at zero pressure corresponds to $T \gtrsim 3T_c$, the measured resonance frequency and width are within 10% from the prediction of the model. When temperatures approach T_c the deviation increases and at T_c the resonance width is twice larger than expected. In this temperature range evidently the interaction between the two legs of the fork becomes important and probably the surrounding of the fork (which here includes another fork less than 1 mm away) also influences the result. Thus we can conclude that the simple hydrodynamic model presented here describes reasonably well the behavior of the fork in normal ^3He but is not sufficient for exact scaling of a temperature calibration from one pressure to another, especially in the regime of large viscous penetration depth close to T_c .

7. TUNING FORK IN ^4He

Our measurements in liquid ^4He have also been performed in two different setups. In both cases the forks²⁸ are partially inside their original cans, only a hole is ground in the can to provide a connection between the fork and the liquid in the ^4He sample container. The temperature is determined from the saturated vapor pressure. In the first setup the LHe temperature vacuum parameters of the fork are $f_{0\text{vac}} = 32708$ Hz and $\Delta f_{\text{vac}} = 0.4$ Hz. In the second setup a fork is used with $f_{0\text{vac}} = 32709.97$ Hz and $\Delta f_{\text{vac}} = 0.06$ Hz.

The resonance frequencies of the two forks are shown in Fig. 11 as a function of temperature. In liquid ^4He above the superfluid transition the density changes faster than the viscosity. Thus, the resonant frequency is more useful for thermometry. Indeed the measured resonant frequency is reminiscent of the inverse of the well-known liquid density, with a maximum in the density just above the superfluid transition T_λ . However, a

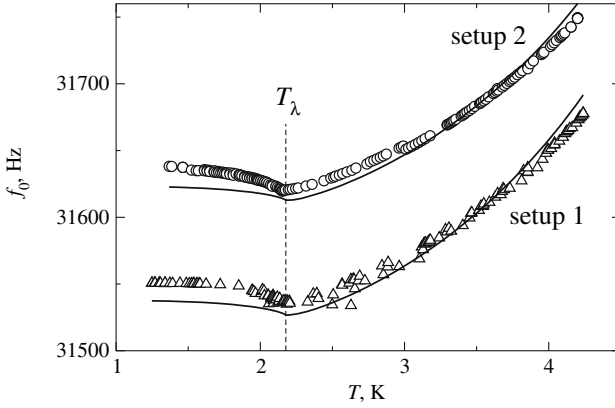


Fig. 11. Resonance frequencies of two quartz tuning forks in liquid ^4He at saturated vapor pressure, measured in two different setups. The symbols represent experimental data. The lines have been fit to the data at $T > T_\lambda$, using Eq. (20) with β as fitting parameter and $B=1$. The fit gives $\beta=1.39$ for setup 1 and $\beta=1.27$ for setup 2. The data on the physical properties of liquid ^4He are from Ref. 29.

fit of the measured frequency in the normal phase to Eq. (20) shows systematic differences which so far remain unexplained. In normal ^4He the viscous penetration depth δ is of sub-micron size. Thus the influence of the small viscous term in the added mass cannot be reliably distinguished in the presence of the rapid variation of the liquid density. Therefore, in Fig. 11 the value of B is fixed to 1 and the only fitting parameter is β .

Below T_λ we plot the extrapolation of Eq. (20) in Fig. 11, assuming a simple two-fluid-model interpretation. The interaction of the normal and superfluid fractions via the possible existence of quantized vortices is neglected. The inertial contribution to the effective mass is attributed to the whole fluid, while the viscous contribution is assumed to originate only from the normal fluid component. Thus $(f_{0\text{vac}}/f_0)^2 = 1 + \beta\rho/\rho_q + BS/(V\rho_q)\sqrt{\eta\rho_n/\pi f_0}$, where ρ_n is the density of the normal component. In view of the systematic difference between the fit and the measurements in the normal phase, the extrapolation to $T < T_\lambda$ is reasonable.

In Fig. 12, we plot the same data once more with $[(f_{0\text{vac}}/f_0)^2 - 1]/\beta$ on the vertical scale versus temperature. Now the two sets of data are reduced on the same temperature dependence, which is mainly that of the total liquid density ρ . The nice agreement in this plot lends support to the model expressed by Eq. (20) and to the extracted values of β for the two forks, derived by fitting their data separately to Eq. (20) at temperatures

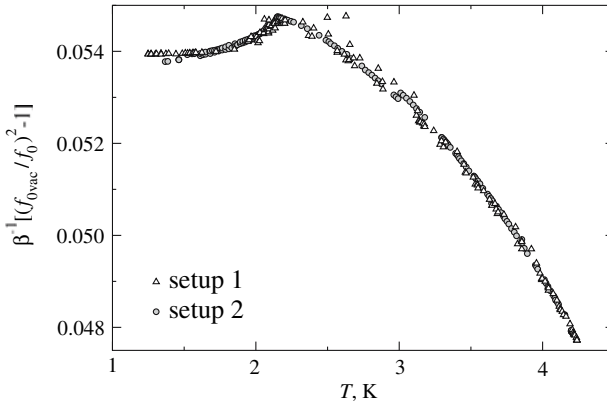


Fig. 12. Scaled resonance frequencies of two quartz tuning forks in liquid ^4He at saturated vapor pressure. Plotted in this way both sets of data from Fig. 11 coincide. The quantity on the vertical axis is $[(f_{0\text{vac}}/f_0)^2 - 1]/\beta$, which can be considered an “effective” value of the density ρ/ρ_q .

$T > T_\lambda$. Similar to the ^3He results in the previous section, we obtain rather different values for the β factors of the two forks ($\beta = 1.39$ and 1.27 , Fig. 11). These β values are larger than those from the ^3He measurements, presumably owing to the can around the fork. Interestingly in Fig. 12, the resonant frequency, when scaled with the relevant β value, looks promising as a calibration for thermometry in ^4He at $T > 1.5\text{ K}$.

In Fig. 13, the resonance widths of the two tuning forks are shown. Above T_λ the viscosity of liquid ^4He is not a strong function of temperature and a fit of the data to Eq. (21), using \mathcal{C} as a fitting parameter, works reasonably well. Thus it is interesting to compare the extrapolation of the fit to the experimental data in the temperature regime $T < T_\lambda$. In the extrapolation we use the same model of non-interacting normal and superfluid components. The resonance width is only associated with the normal component and thus in Eq. (21) we replace ρ with ρ_n . Remarkably, the two forks follow nicely the extrapolated dependence in the superfluid regime, in one case down to 1.8 K and in the other to 1.4 K .

An intriguing question is whether any contribution in these results can be attributed to vortex generation and mutual friction.³⁰ From earlier measurements with vibrating wires, grids, and spheres it is known that extra damping occurs in superfluid ^4He even at low drive from the interaction of the normal and superfluid components in the presence of quantized vortices, from mutual friction losses. In ^4He vortices are easily pinned on surfaces as the vortex core is of atomic size and any surface

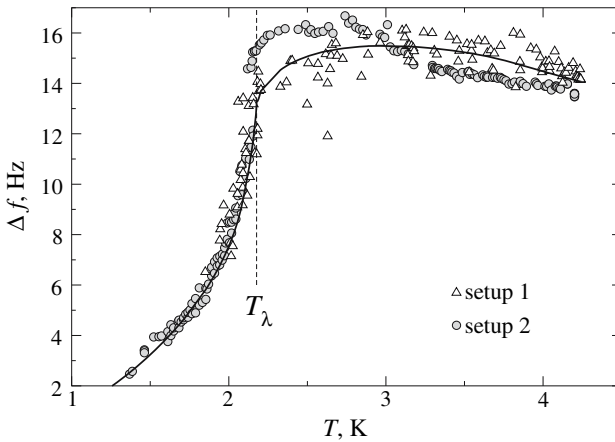


Fig. 13. Resonance widths of two quartz tuning forks in liquid ${}^4\text{He}$ at saturated vapor pressure. The symbols represent the experimental data and the line is a fit of the data from setup 1 at $T > T_\lambda$ to Eq. (21) using C as fitting parameter. The fit gives $C = 0.90$. The fit to the setup 2 data is almost identical to the one shown and gives $C = 0.88$. The data on the physical properties of liquid ${}^4\text{He}$ are from Ref. 29.

becomes sufficiently rough for pinning. Thus the surface of the vibrating sensor might be loaded with pinned remanent vortices. These vortices could originate from thermal counterflow produced in a rapid cool down through T_c , from some other source of residual flow in the system, or if the oscillating object has been driven previously in the superfluid state at velocities above some critical value.

In the present measurements shown in Fig. 13, the amplitude of the fork current was always kept low (typically below 120 nA). This current corresponds to velocities less than 1.5 cm/s, which is below the typical critical velocity in ${}^4\text{He}$ of order 4–5 cm/s. Additional tests were performed when the forks were driven hard enough so that nonlinear response could be seen and vortices should have been created. After the drive was reduced back to low level the width also returned to the original value shown in Fig. 13 without hysteresis. This stability in the response is quite unlike the usually observed differences between “virgin” and “trained” responses of a vibrating grid, for instance.³¹ If this stability of the forks can be reliably reproduced and especially if it persists down to lower temperatures, then the quartz tuning fork might become a useful thermometer for superfluid ${}^4\text{He}$ which is not troubled by “vortex layer” problems.

8. CONCLUSIONS

The quartz tuning fork is a robust and easy-to-use sensor in cryogenic environments. In view of the results in Fig. 7, it appears to be a useful secondary thermometer for superfluid ^3He research. It requires less work and know how to implement and operate than any other of the currently available methods in the superfluid ^3He temperature regime. Its response is well described at low excitation in the linear drive regime in terms of our hydrodynamic model which includes fitting parameters with a physical origin. More statistics on different forks are needed to decide whether simple means can be worked out to fix the parameter values and the calibration of the device as a thermometer. For such tests the forks should be adequately thermally cycled and preselected based on their LHe temperature resonance widths Δf_{vac} in vacuum. The important physics, which should be explored with the quartz tuning fork, lies at the lowest temperatures in the ballistic regime, both in $^4\text{He-II}$ and $^3\text{He-B}$, where the interaction of the fork with quantized vortices should be investigated.

EPILOGUE: Dedication to Frank Pobell

Oscillating devices immersed in a bath of liquid He were an important element in Frank Pobell's research. He is remembered for his passionate mission to reach ever lower temperature records. A controversial element in this quest was thermometry. The vibrating wire resonator was and still is the best thermometer for the $T \rightarrow 0$ limit in $^3\text{He-B}$. To explore the limits of this device, he studied in many papers the nonlinear response and dissipation in different wire materials down to below 1 mK in vacuum. He discovered that even metals display slow heat release from defect structures, which relax similar to the tunneling model of two-level systems in glassy amorphous materials.²² These measurements should now be repeated for the quartz tuning fork.

The senior members among the authors of this report remember Frank from this time as an extremely focused and industrious researcher. He was a visitor in the Low Temperature Laboratory for two months during the spring term of 1991. One of us (MK) was sharing the office room with him. He was working from early morning until late evening without break on his administrative chores, writing his research reports, and examining the manuscripts submitted for publication in JLTP. We were so impressed by this diligence and the steady flow of new results. An excellent example is his book²⁰ "Matter and Methods at Low Temperatures," which he had just completed and which appeared later in the same year. This book is still gratefully used as the best text book for our courses in

low temperature physics. East of Germany Frank is remembered (LS and PS) for his help and support to the low temperature community behind the iron curtain before it was lifted in 1989. This special relationship has continued over the years, an example was Frank's co-chairmanship of the LT21 Conference in 1996 in Prague.

ACKNOWLEDGMENTS

This research is supported in part by the EU research program ULTI-4 (RITA-CT-2003-505313), by the Institutional Research Plan AVOZ10100520 and the Czech Grant Agency under grant GACR202/05/0218, by the Slovak Grant Agency VEGA under grant 2/6168/06 and by the SAS under grant CE I-2/2003.

REFERENCES

1. E. P. Eernisse, R. W. Ward, and R. B. Wiggins, *IEEE Trans. Ultrason. Ferroelectr. Freq. Control* **35**, 323 (1988) – a survey of quartz resonator sensor technologies.
2. D. O. Clubb, O. V. L. Buu, R. M. Bowley, R. Nyman, and J. R. Owers-Bradley, *J. Low Temp. Phys.* **136**, 1 (2004).
3. J. Rychen, T. Ihn, P. Studerus, A. Herrmann, K. Ensslin, H. J. Hug, P. J. A. van Schendel, and H. J. Güntherodt, *Rev. Sci. Instr.* **71**, 1695 (2000).
4. M. Niemetz, H. Kerscher, and W. Schoepe, *J. Low Temp. Phys.* **126**, 287 (2002). [W. Schoepe, *Phys. Rev. Lett.* **92**, 095301 (2004)]–electrically driven magnetically levitated oscillating sphere in $^4\text{He-II}$.
5. H. A. Nichol, L. Skrbek, P. C. Hendry, and P. V. E. McClintock, *Phys. Rev. Lett.* **92**, 244501 (2004). [*Phys. Rev. E* **70**, 056307 (2004)]–electrically driven oscillating grid in $^4\text{He-II}$.
6. H. Yano, A. Handa, H. Nakagawa, K. Obara, O. Ishikawa, T. Hata, and M. Nakagawa, *J. Low Temp. Phys.* **138**, 561 (2005)–vibrating wire resonator in $^4\text{He-II}$.
7. D. I. Bradley, D. O. Clubb, S. N. Fisher, A. M. Guénault, R. P. Haley, C. J. Matthews, G. R. Pickett, V. Tsepelin, and K. Zaki, *Phys. Rev. Lett.* **95**, 035302 (2005). [*ibid.* **96**, 035301 (2006)].
8. D. I. Bradley, *Phys. Rev. Lett.* **84**, 1252 (2000).
9. J. Martikainen, J. Tuoriniemi, T. Knuuttila, and G. Pickett, *J. Low Temp. Phys.* **126**, 139 (2002)–vibrating wire resonator in $^3\text{He} - ^4\text{He}$ solution.
10. K. Karrai and R. D. Grober, *Tip-sample distance control for near-field scanning optical microscopes*, in *Near-Field Optics*, M. A. Paesler and P. T. Moyer (ed.), *Proc. SPIE* **2535**, 69 (1995).
11. K. Karrai, lecture notes (2000) at <http://www.nano.physik.uni-muenchen.de/publikationen/Preprints/p-00-03.Karrai.pdf>
12. L. D. Landau and E. M. Lifshitz, *Fluid Mechanics*, Pergamon Press, Oxford, UK (1987).
13. L. M. Milne-Thomson, *Theoretical hydrodynamics*, Dover Publications, New York (1996); H. Lamb, *Hydrodynamics*, Dover Publications, New York (1945).
14. J. E. Sader, *J. Appl. Phys.* **84**, 64 (1998).
15. E. N. Martinez, P. Esquinazi, and J. Luzuriaga, *Am. J. Phys.* **58**, 1163 (1990).
16. M. Morishita, T. Kuroda, A. Sawada, and T. Satoh, *J. Low Temp. Phys.* **76**, 387 (1989).
17. C. B. Winkelmann, E. Collin, Yu. M. Bunkov, and H. Godfrin, *J. Low Temp. Phys.* **135**, 3 (2004).
18. J. Jäger, B. Schuderer, and W. Schoepe, *Physica B* **210**, 201 (1995).

19. V. D. Arp and R. C. McCarty, *The Properties of Critical Helium Gas* Technical Report, University Oregon (1998); R. D. McCarty, *Thermophysical Properties of Helium-4 from 2 to 1500 K with Pressures to 1000 atm*, Technical Note 631, National Bureau of Standards, Gaithersburg, Maryland (1972).
20. Frank Pobell, *Matter and Methods at Low Temperatures*, Springer, Berlin, 2nd ed (1996).
21. P. Skyba, J. Nyéki, E. Gažo, V. Makroczyová, Yu. M. Bunkov, D. A. Sergackov, and A. Feher, *Cryogenics* **37**, 293 (1997).
22. R. König, P. Esquinazi, and F. Pobell, *J. Low Temp. Phys.* **90**, 55 (1993).
23. The fork used in the measurements at 29 bar pressure was manufactured in Japan and was obtained from RS Company under stock number 472-1161, brand Fox Electronics and manufacturer's part number NC26. The fork used in the zero pressure measurements was manufactured in Taiwan and was obtained from RS Company under stock number 226-1437, brand C-MAC Frequency Products and manufacturer's part number A103C.
24. A. I. Ahonen, M. Krusius, and M. A. Paalanen, *J. Low Temp. Phys.* **25**, 421 (1976); P. J. Hakonen, M. Krusius, M. M. Salomaa, R. H. Salmelin, J. T. Simola, A. D. Gongadze, G. E. Vachnadze, and G. A. Kharadze, *J. Low Temp. Phys.* **76**, 225 (1989).
25. D. C. Carless, H. E. Hall, and J. R. Hook, *J. Low Temp. Phys.* **50**, 583 (1983).
26. E. R. Dobbs, *Helium Three*, Oxford University Press, Oxford, UK (2000).
27. P. R. Roach, Y. Eckstein, M. W. Meisel, and L. Aniola-Jedrzejek, *J. Low Temp. Phys.* **52**, 433 (1983).
28. In setup 1 the same type of fork was used as in ^3He measurements at 29 bar pressure.²³ In setup 2 the fork was made in China by Fronter Electronics, product number DT26.
29. R. J. Donnelly and C. F. Barenghi, *J. Phys. Chem. Ref. Data* **27**, 1217 (1998).
30. R. J. Donnelly, *Quantized vortices in Helium II*, Cambridge University Press, Cambridge (1991).
31. W. F. Vinen, L. Skrbek, and H. A. Nichol, *J. Low Temp. Phys.* **135**, 423 (2004).